MEASUREMENT OF THE SPATIO-TEMPORAL DISTRIBUTION OF ARCS DURING VACUUM ARC REMELTING AND THEIR IMPLICATIONS ON VAR SOLIDIFCATION DEFECTS

Joshua Motley[1], Kanchan Kelkar[2], Paul King[1], Matt Cibula[1], and Alec Mitchell[3]

[1]Ampere Scientific, 1546 SW Industrial Way, Albany, OR 97322, USA
[2]Innovative Research, LLC, 3025 Harbor Lane North, Suite 225, Plymouth, MN 55447, USA
[3]Univ. British Columbia, 2329 West Mall, Vancouver, BC, Canada V6T 1Z4

Keywords: Vacuum arc remelting, electro-slag remelting, solidification, computational fluid dynamics, modeling segregation, electric arc, defects

Abstract

The behavior of vacuum arcs during VAR processing is known to impact product yield and contribute to ingot defects. For example, it has been shown that constricted arcs during the processing of segregation prone nickel-based alloys can lead to defects in ingots. Despite this knowledge, the role of arc distributions in VAR processing has not been considered in controlling the furnaces. In addition, computational models of the process have typically assumed that the arc provides an axisymmetric, Gaussian heat input to the ingot, while acknowledging that this is the biggest unknown variable. Here we present the theory behind *VARmetric*^{TM} and present analyses of the spatio-temporal arc distributions measured on a production VAR furnace. We then use the measured axisymmetric arc distributions to provide updated boundary conditions for solidification of the ingot to investigate the implications of the changing distributions on solidification and the relationship between arc distributions and defects.

Introduction

Vacuum arc remelting (VAR) is essential in the processing of high strength alloys, such as Ni-based alloys, to increase homogeneity and dissolve defective material, producing ingots with a highly uniform chemical composition. The production of larger Ni-alloy ingots is desired for large engine and power turbine parts. In these cases, high strength defect free ingots are required while in some alloys, defects are more prevalent at larger diameters.

The fluid flow within the melt pool can alter the local chemistry and solidification causing changes in the ingot composition. These changes manifest as defects such as white spots, freckles, or tree-rings. White spots are solute lean regions and result from un-melted particles that can originate from fall-in from the shelf or crown [1]. Freckles are elongated grain structures enriched with Nb, Mo, and Ti, appearing within the ingot mid radius and center. The freckle formations occur when there is a density inversion within the solute which promotes convection within the mushy region [2]. When the buoyancy forces of the enriched lighter solute exceed the resistance to flow provided by the solidifying dendrites, the solute rich liquid plumes upward and the enriched flow solidifies as freckles. Tree-ring defects form when flow conditions change within the mushy zone. The fluctuating flow conditions cause perturbations in the solidification front, temporally transitioning from columnar to equiaxial grain structure [3]. Their occurrence can be reduced by maintaining consistent and unperturbed mass and heat flow conditions within the melt pool.

The reduction and ultimately elimination of these defects is critical to producing large diameter ingots. The prevention of these defects can be achieved by control of the melt pool solidification conditions [4]. Within the mushy region, liquid flows between the solidified dendrites and is affected by the permeability of the dendritic structures [5]. The permeability is non-isotropic and flow through the interdendritic layer is influenced by the orientation of flow with respect to gravity [6]. The use of a critical Rayleigh number (Ra) has been proposed as a criteria for freckle formation [2]. Segregation of elements, such as Nb, within the mushy zone generates an inverted density gradient. Freckles can be avoided by keeping the solidification rates below the critical values. The resistance to flow is controlled by the geometry and density of dendrites within the mushy zone. The proper critical length scale for use of the Ra number has been debated, however there is a general consensus that it should be related to the primary and secondary dendrite spacing [5]–[7].

To date, one of the least known input parameters to solidification models, which are used to predict defect formation, is the distribution of current throughout the arc and, consequently, the heat flux at the liquid boundary at the top of the ingot. The arc is composed of individual cathode spots which move across the electrode surface in a semi-random nature. The movement of cathode spots are short-lived and extinguish and reignite locally in adjacent space at a velocity of 1-10 m/s. Each arc contains clusters of cathode spots with each cathode spot carrying 79-190 amps [8]. Studies on the energy flow show that only 45-65% of the electrical current passes from the electrode to the melt pool [9]. The remaining current is lost through the plasma between the crucible wall and electrode. In a diffuse arc mode, the cathode spots are generally well dispersed across the electrode surface. This provides a macro-uniform heat input into the melt pool. Changes in electrode or gas composition within the arc gap can concentrate the cathode spots into a constricted mode. In this mode the arc is highly localized and contains higher densities of cathode spots. Constricted arcs are known to reduce electrical efficiency and subsequently lead to lower melt rates.

The position and movement of the cathode spots is difficult to observe in industrial VARs due to the geometry of the systems and the intense luminosity and heat produced by the arc. The motion and position of the arcs are typically monitored using video cameras aimed down the annulus between the electrode and furnace wall. This provides a small visual window revealing a small melt pool region and light intensity that emerges from the annulus between the electrode and crucible wall. Attempts at inferring the motion and distribution of arcs in an industrial VAR have been made by inspecting the luminosity intensity and periodicity. The observed cathode spot movements have been described as an ensemble of motion with a centroid exhibiting periodic behavior over a sufficient time period, 20-60 seconds [10]. Simulations of arcs on cold cathode surfaces indicate they move radially from the center of the electrode outward, with the azimuthal rotation either clockwise or counter clockwise [11]. Measurements of the magnetic flux have also been used to reconstruct the averaged centroid of the cathode spots [12]. Similar magnetic flux measurements of the arc have indicated arcs that tend to rotate around the vertical axis of the furnace with similar periods, along with well centered and more complicated semicircular arc patterns [13].

In this work we present various simulations incorporating time averaged transient heat and current boundary conditions due to the dynamic arc motions. These distributions represent the time averaged radial distributions observed during industrial melts performed at ATI Specialty Alloys. The effect on the melt pool and solidification due to the different time averaged ensemble of motions are modeled.

Experimental Basis

A *VARmetric*^{TM} system [14], [15] was mounted to the exterior shell of an industrial VAR to measure the magnetic fields emanating from the electric arcs simultaneously with other furnace measurements such as current and voltage. The system consisted of 3-axis Hall effect sensors arrayed around the

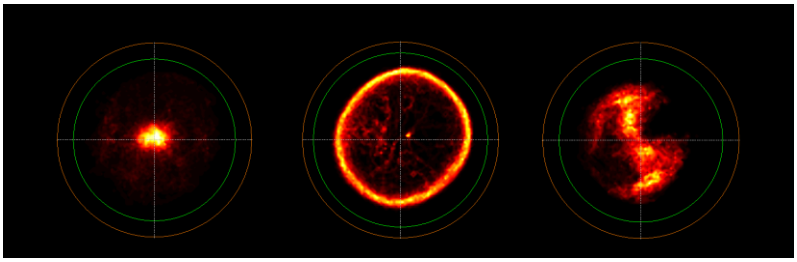

Figure 1. 3 distinctly different distributions measured during the production of a Ti ingot. Courtesy of Woodside et al.

furnace shell to continuously acquire data near the arc gap as it moves up through the furnace. The magnetic fields were used to calculate the centroid of the arc distribution using methods previously reported [16]. Data on the arc locations was collected during the final melt of a Ti-alloy. Although the arc position measurements were taken during the melting of titanium, the arc distributions are expected to be similar to Ni-alloy melts [17], [18]. Figure 1 plots several measured arc distributions, taken within the melting of the same ingot during steady state, with no apparent variation in the standard signals. Each of these distributions lasted more than 720s and were separated by a period of time ranging up to 30 minutes. For the purposes of this work, we consider the 'Center' and 'Ring' distributions in particular since these are the only distributions that can be modeled as axisymmetric. In regards to the 'Center' distribution, this particular plot represents either a constricted distribution in the center of the electrode or a diffuse distribution covering the entirety of the electrode surface. Without further analysis of the measurements and measurement error, we can not determine the difference between these two unique modes. Since the solidification and segregation of Ni-alloys is more sensitive to processing parameters, we chose to simulate the effect of the arc distributions on Ni-alloy 718 utilizing the assumption that time averaged arc distributions from previous measurements could be applied.

The radial and angular position of the arc are measured at 120 Hz and used to examine collections of arc distributions in 5-35 minute intervals. The arc radial position data was binned in 12.7 mm increments and histograms were used to plot the arc distribution over the interval. The three different measured distribution examples are shown in Figure 2. In this case, the choice of 40 mm for the current density full-width half-max is somewhat arbitrary, because it is not known if the arc is constricted or diffuse over the surface of the ingot. It is important here to note that this process treats the data as purely axisymmetric, which is often not the case, but the lack of a robust 3D VAR solidification model necessitates this approach. Figure 3 shows how the measured data was treated as axisymmetric. Rather than use the arc location as measured relative to the furnace, the displacement from the mean during the interval was taken. To set up the model, each measured arc centroid was approximated to be a Gaussian distribution of current density with a full half-width max of 40 mm. The sum of all arcs over a fixed time interval was taken to generate a Gaussian function, normalized to the surface area.

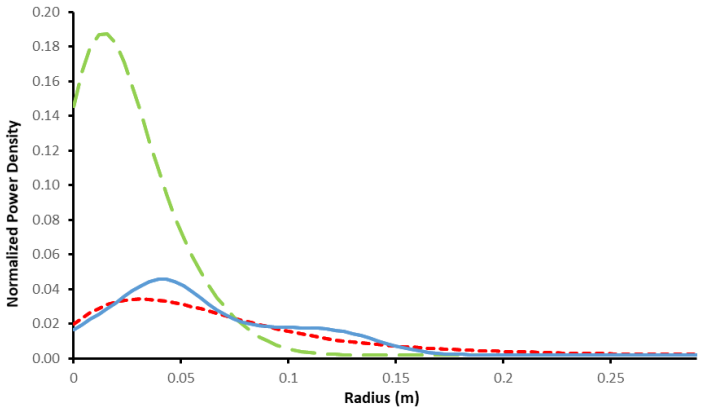

Figure 2. Examples of axisymmetric current density distributions calculated from magnetic field measurements using VARmetric™.

Simulations were completed using a modified version of MeltFlow-VAR. MeltFlow-VAR is a multiscale numerical simulation package developed for VAR. It provides a computational solution for mass, momentum, heat transfer, phase change, and thermal history. The software provides a means of examining metallurgical structure and probability of defect formation due to changing boundary conditions. Metallurgical properties for Ni-alloy 718 were used for this study due to its wide use and highly studied properties. The model used axisymmetric boundary conditions about the center axis. The boundary condition at the pool surface includes the current

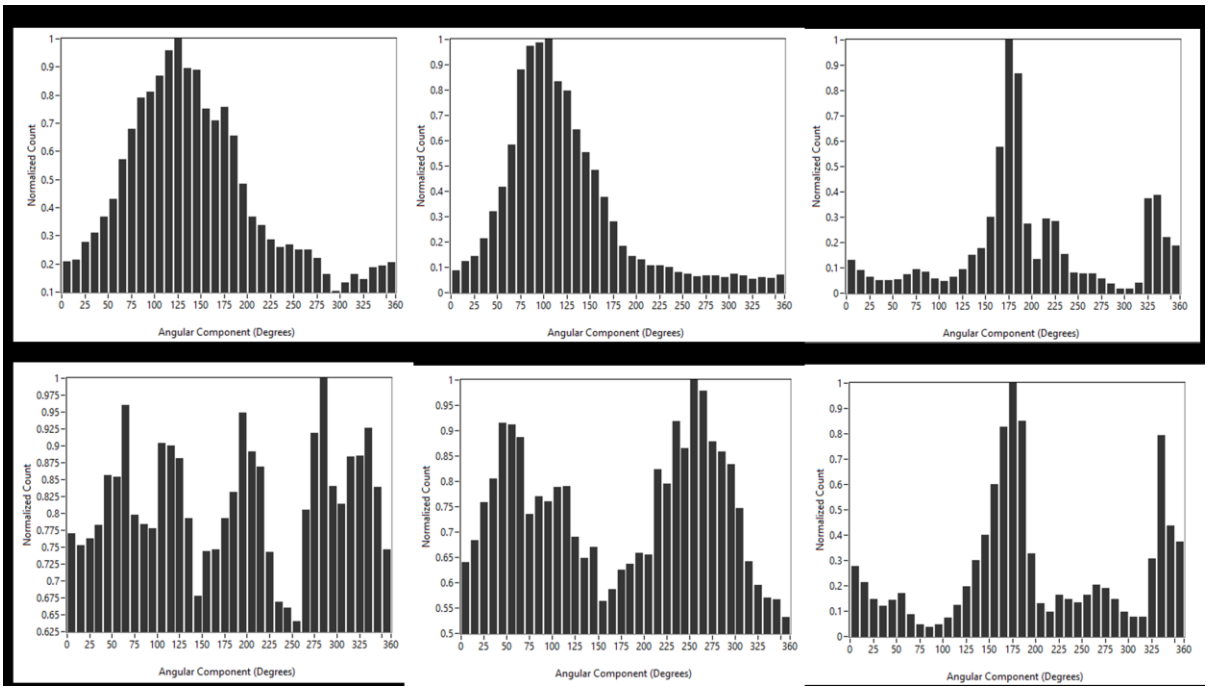

Figure 3. Angular distributions of arc locations measured over 30 minutes for 3 example intervals in the same melt. The average location of the arc during each period was offset from the center of the furnace, indicated by a single peak on the upper row of plots. The displacement of the centroid from the mean was utilized to model the data as axisymmetric. From left to right, the mean arc location was X, Y, Z. Even after the correction, the bottom set of angular distributions indicate that the data is not truly axisymmetric.

density and heat provided by the arc, and radiative heat loss. Heat transfer through the sides incorporates an ingot shrinkage factor that determines the contact resistance. Momentum transfer is solved for using the two equation k-ε for turbulent flow. The Rayleigh number is calculated in Equation 1, where the interdendritic length scale is '*l*', given by the effective permeability with respect to gravity [19]. The characteristic length scale of the dendrite spacing is calculated by the method proposed by Auburin *et. al* [5].

$$\mathrm{Ra} = \frac{g\left(\frac{\partial \rho}{\partial T}\right)\left(\frac{\partial T}{\partial x}\right)}{\mu\left(\frac{k}{\rho C_p}\right)} l^4 \tag{1}$$

The transient current density and heat flux boundary conditions for the top of the pool follow an axisymmetric Gaussian distribution shown in Equation 2, where σ is the arc spread factor, u_{center} is the mean center of the distribution, and R_{ingot} is the ingot radius. The arc spread factor and center was varied with time during the simulations allowing for the effects of arc dynamics and time averaged distributions, similar to those observed experimentally by *VARmetric*^{TM}, to be studied.

$$j(r,t) = j_o e^{-3\left(\frac{r - u_{center}(t)}{\sigma(t)\, R_{ingot}}\right)^2} \tag{2}$$

All melts were simulated with a total current of 6 kA, at constant melt rate of 250 kg/hr, for 526 minutes. The electrode diameter was 440 mm with a final ingot diameter of 500 mm. The electrode voltage was set to 25 V. The partition of total current to the melt pool was 0.6 for all

cases. Since the objective was to study the time-varying arc implications during steady state, the simulations did not include initial transient or hot top melting conditions, and the only input variable that was altered during the simulation was the arc distribution, which also modifies the normalized heat flux input to the melt pool. The ingot was melted using a centered diffuse arc ($\sigma = 5$) for the first 300 minutes to allow the melt pool to reach a steady state so any effects were independent from the startup dynamics associated with heat transfer to the bottom of the pool. After 301 minutes the arc center and spread factor were changed and held constant for a set time, then returned to the original diffuse distribution. The arc parameters used in the simulations are shown in where Figure 4 plots the corresponding distributions. Since the model is axisymmetric, the offset arc condition represents a constricted arc rotating at the mid-section of the pool radius. The diffuse condition, with a large σ, is representative of a diffuse arc condition. The centered arc with a narrow distribution represents a constricted arc focused in the center of the melt pool. All arc conditions were normalized to the furnace current and power.

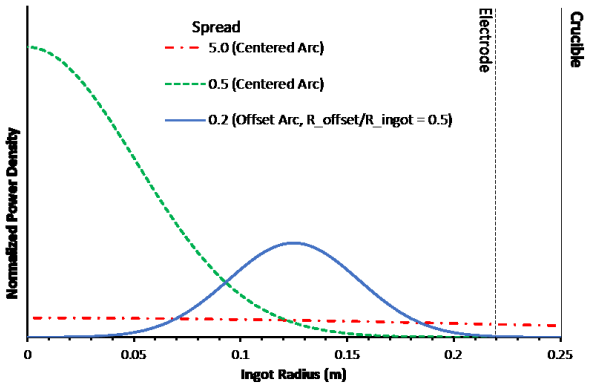

Figure 4. Axisymmetric arc power distributions used for transient arc boundary conditions simulations using MeltFlow-VAR.

Results & Discussion

It took about 30-40 minutes for the pool to approach steady state after the change from diffuse to constricted arc conditions. Figure 5 shows the liquid velocities and the liquid fraction for the centered diffuse, center focused, and the constricted offset distributions for the 30 minute interrupt cases. In all cases the pool volume increased when the arc is deviated from the diffuse condition. This could be due to melt back from the shallower pool and increase in flow velocity. For the centered arc this is likely due to the focused current density entering the center of the pool. The increase in downward flow along the outer edges of the pool results in the mushy zone becoming depressed and broadening. The depth of the melt pool at which solidification begins increased from 160 mm below the pool surface, to 190 and 200 mm for both the offset and centered cases. Zanner *et. al*, produced simulations that predicted the pool to decrease in volume and for the solidification time to increase for the case of a constricted arc [20]. The discrepancy in results may be attributed to the constant melt rate across the electrode, which may not be radially constant with varying the arc conditions. It is known that the mode the arc is operating in affects the melt rate and likely the distribution of metal transfer to the pool. Simulations of a 3D rotating arc and melt pool indicate that the motion and heat input from the arc generates considerable melt back in the mushy zone [21]. Diffuse modes have higher electrical efficiencies and higher melting rates [22]. For these studies the melt rate and efficiencies were kept the same for all conditions.

The liquid flow profile is greatly influenced by the arc distributions chosen here. In the diffuse condition the flow is primarily driven by buoyancy forces. The offset arc condition generates two flow cells shown in Figure 5. This is due to the greater Lorentz forces generated by the increase in current density, especially for the centered focused arc. The max pool velocity increases from 3 mm/s to 9 mm/s for the offset arc, and to 17 mm/s for the center focused arc. The maximum

velocities for the two interrupt cases is about 50-60 mm below the pool surface nearest the walls. In all cases, after the interruption, the pool returns to a shallower state.

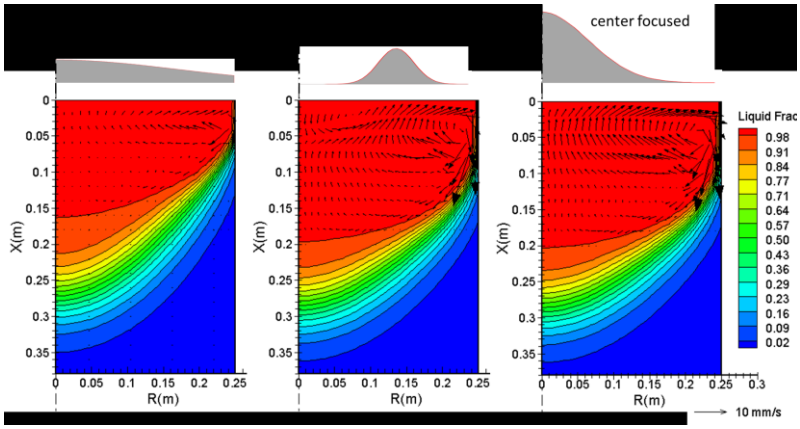

Figure 5. Pool liquid fraction and fluid velocities during the diffuse and interrupt conditions. Interrupt began at t = 301 mins and were maintained for 30 minutes. All plots shown at t = 330mins.

Fluctuations in pool depth have already been linked to certain defect formations. For example, tree-ring formation can occur as the solidification front adjusts to the transient conditions at the pool surface [3]. Variations in the solidification front cause irregularities in the growth of dendrite tips and promotes segregation [22]. Also, one proposed mechanism for white spots is the fragments from crown or shelf reentering the melt pool [1]. Simulations show these particles may not completely dissolve in the deeper cool liquid if they are above 3-6 mm in diameter [23]. Such remelting of the crown may occur if the arc transitions between offset and centered modes. Finally, one of the consequences from the increased liquid velocities is the increased likelihood of dendrites breaking and reentering the liquid pool, which has been a proposed mechanism for white spot formations [22].

Figure 6 shows the Rayleigh number during solidification for each other cases, at a specified solid fraction of 0.5. It is believed that the theoretical critical Rayleigh number for prevention of freckles should be kept below 1, however studies show that the critical Rayleigh number for IN718 is 0.2-0.6 [5], [6]. From a qualitative analysis the higher Rayleigh numbers indicate greater chances for freckle formation. The Ra numbers in the midsection increased from 0.2 to 0.32.

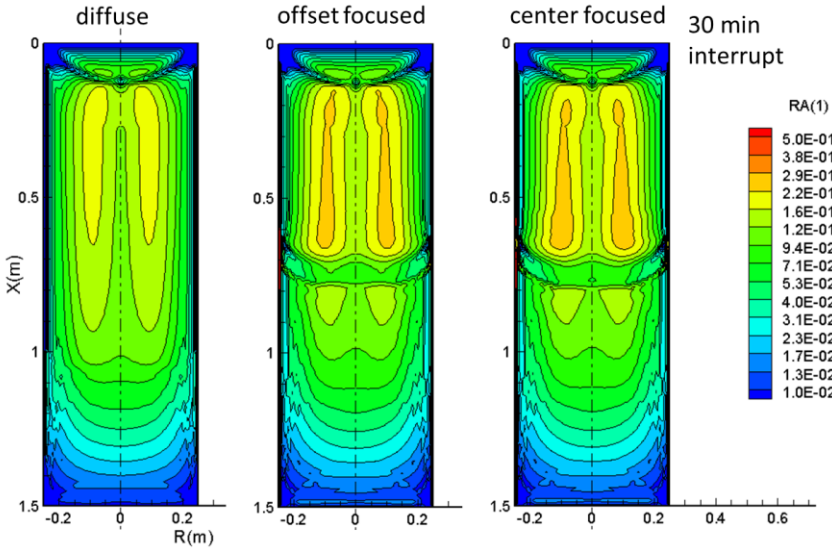

Figure 6. Rayleigh numbers in the interdendritic region at a solid fraction of 0.5. The transition from the arc conditions is evident and influences the remaining melt after returning to diffusive conditions. The Ra number is strongly affected near the walls where solidification is strongly influenced by the heat flux to the crucible wall.

The longitudinal variation in Rayleigh number is evident for both short and long duration interruptions. Where longer interruptions have larger effects to the solidification of the ingot and subsequently increased chances for freckle formation in the midsection.

The onset of the interruption affects the flow dramatically and reduces the Ra number. The effects of the interruption are seen later in the history after the diffuse condition is resumed. This can be attributed to the melt pool reshaping to a narrower profile with higher solidification angles.

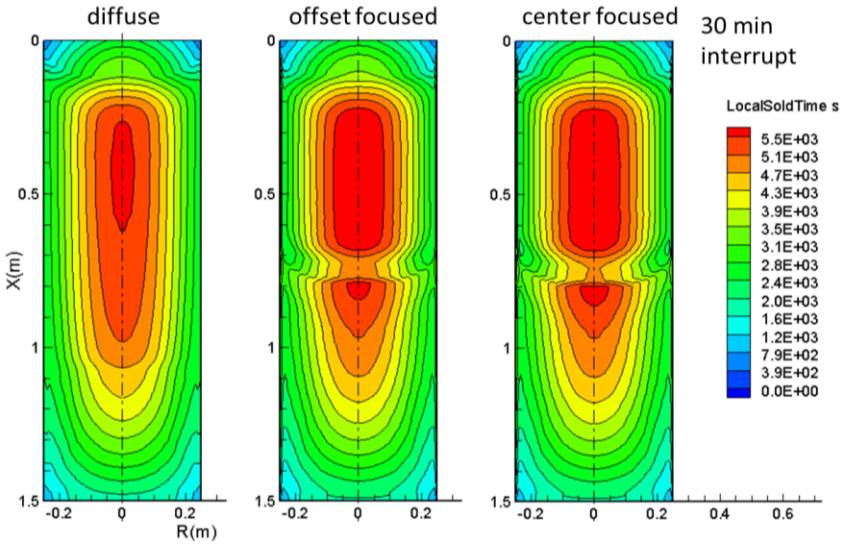

Figure 7. Solidification time at a solid fraction of 0.5. Interestingly, after the arc is returned to a diffuse state from either interrupt condition, the LST is permanently broadened across the ingot. The LST is also reduced during both interrupts.

During the onset of the interrupt, the melt pool broadens and becomes deeper while the mushy zone decreases in vertical thickness. After the interrupt is finished and diffuse condition is returned, the pool goes through a rapid reshaping with the solidification angle in the mid-section reaching a maximum value higher than the steady state diffuse solidification angle. This is due to the heat transfer being greater near the crucible walls causing the regions nearest the wall to solidify quicker. After about 60 minutes, the pool returns to similar conditions to before the interruption for the 30-minute interrupts. However, the Ra number reaches a maximum and remains high well after the return to diffuse conditions.

One main effect of the interruptions is to decrease the local solidification time (LST). Figure 7 shows the difference in solidification time for the different long interrupt conditions. For both interrupt conditions the local solidification time decreases during the interrupt. The increase in heat flow carried by the fluid decreases the temperature gradient and the solidification front speed. The increase in recirculating flow due to the interrupts well above the mushy zone may cause more energy to be lost at the crucible wall, which decreases the amount of heat flowing along the mushy zone interface. After the flow returns to steady state under diffuse conditions the width of LST is broadened compared to the purely diffuse melt. The effect of an interrupt is carried through the entire history of melt after the interrupt. The influence on

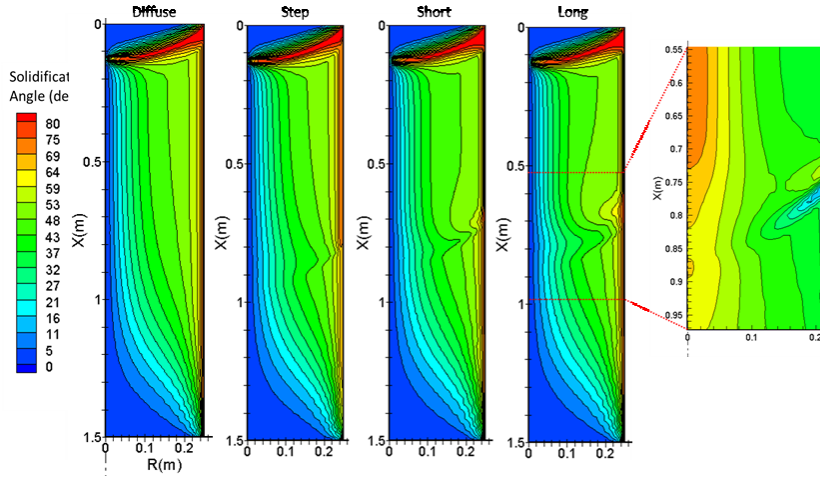

Figure 8. Cooling rate at the near liquidus temperature. Left to right: diffuse only, diffuse-offset, diffuse-offset (10 min)-diffuse, and diffuse-offset (30 min)-diffuse. Notice that the perturbations from the diffuse case are more pronounced for the short and long interrupts than for the step change.

the LST is most drastic near the crucible wall and mid-section.

A simulation with a single step change from diffuse to offset was used to examine if the onset of the interruption condition or return to diffuse conditions lead to the broadened features seen in the thermal history. This simulation used the same conditions as the offset arc but was held for the rest of the melt instead of returning to diffuse conditions. Figure shows the solidification angle for the 4 cases, along with the speed of the solidification front for the long interrupt case. For the duration of the interrupt condition the solidification angle is reduced in the midsection. After the interrupt the solidification angle increases near the crucible walls where the heat transfer to the wall is highest, and slowly returns to angles similar to the diffuse case. However, the step condition shows that the angle decreases, but when the offset is maintained the mid-section and center of the pool returns to angles similar to the purely diffuse condition. The solidification angle remains high near the crucible wall for the remaining time of the offset. The solidification speed shown for the long offset shows that the front slows down during the offset, likely due to increase in hot liquid flow near the edge of the pool. After the interrupt condition the heat input near the walls is lower but the momentum continues to drive the fluid. The heat transfer near the wall is still high and the decrease in enthalpy provided by the fluid causes the pool to solidify faster. As mentioned before, these oscillations in solidification speeds increase the likelihood of tree-ring formations. The step condition shows that the pool can maintain steady solidification conditions if the changes in arc dynamics are low frequency. However, it appears that medium time scale variations in arc distributions on the order of 10-30 minutes can greatly influence the solidification and should be avoided, although quicker interruptions are less likely to lead to a change the solidification.

Conclusions

This paper contemplates the effect of arc distributions on solidification characteristics. In particular, if the heat flux at the pool surface is known at every given moment, what is the overall effect of heat flux changes on metal quality? Measurements of arc distributions during VAR melting of titanium were used to develop a heat flux distribution. These distributions were used to model solidification responses for IN718. Although this scenario is a bit contrived, we feel it is instructional in understanding solidification dynamics under axisymmetric assumptions.

To this end, measurements of the arc centroid was performed by using magnetic field measurements. Three different experimentally measured distributions of arcs encountered during industrial melts were presented. Simulations incorporating an axisymmetric time varying gaussian boundary conditions approximating the 3 different arc distributions were performed. The results show that the interruption from diffuse conditions greatly influences the solidification in the outer regions of the ingot. Shorter lasting interrupts such as the 10-minute interrupt condition simulated here influence the solidification less due to the long time it takes to establish new steady state conditions. The interrupt causes long lasting changes to the remaining thermal history which may impact the overall product quality.

Over the course of 4 years of taking industrial data, there have been many observations of time intervals where the arc did not rotate in a circular motion centered on the electrode. For example, an arc could tend to spend more time in a single quadrant for extended periods of time, say 10-60 minutes. The non-symmetric nature of these conditions would lead to non-axisymmetric solidification, the effects of which are hard to predict and outside the scope of this work. In order to fully understand the effects of the richness of the arc dynamics, including centered and off-

centered arcs during VAR processing, a fully coupled 3D model is required. Fortunately, some work on 3D simulations of arcs and their impact on melt pool dynamics have been carried out, but these models lack integration of solidification [17], [21], [24]. In order to fully study the nature of the arc dynamics on the solidification on ingots a full 3D multiscale model is necessary.

Finally, it is apparent in the literature and in these computational efforts that arc dynamics play a significant role in ingot quality. In particular, for highly alloyed ingots, defect formation often is a function of solidification dynamics, dynamics that are controlled in part by the heat flux. Provided that arc positions and, consequently the heat flux measurements, are obtainable through such technologies as *VARmetric*™, integrated simulations or post ingot analysis based upon the true operational conditions could provide an increased measure for the ingot quality in safety critical applications.

Acknowledgements

We are grateful for the insightful discussions with Dr. Rigel Woodside in interpretation of arc distributions and their important role in solidification dynamics. Some or all of this work was supported by the National Science Foundation SBIR Phase I Grant Number 1647655 and the National Science Foundation SBIR Phase II Grant Number 1831255 as well as Business Oregon Grant Numbers C2018096 and C2018335. We are greatly appreciative of the support provided by the National Science Foundation and Business Oregon in support of our efforts.

References

[1] A. Soller, A. Jardy, R. Larue, D. Ablitzer, and G. Reiter, *Proc. 2005 Int. Symp. Liq. Met. Process. Cast.*, pp. 39–48, 2005.
[2] J. R. Sarazin and A. Hellawell, *Metall. Mater. Trans. A*, vol. 19, no. 7, pp. 1861–1871, Jul. 1988.
[3] X. Xu, R. M. Ward, M. H. Jacobs, P. D. Lee, and M. McLean, *Metall. Mater. Trans. A*, vol. 33, no. 6, pp. 1795–1804, Jun. 2002.
[4] J. J. Beaman, L. Felipe Lopez, and R. L. Williamson, *J. Dyn. Syst. Meas. Control*, vol. 136, no. 3, Feb. 2014.
[5] P. Auburtin, T. Wang, S. L. Cockcroft, and A. Mitchell, *Metall. Mater. Trans. B*, vol. 31, no. 4, pp. 801–811, Aug. 2000.
[6] J. Valdes, X. Liu, P. King, C. Cowen, and P. Jablonski, *7th Int. Symp. Superalloy 718 Deriv.*, 2016.
[7] P. Auburtin, S. L. Cockcroft, A. Mitchell, and T. Wang, *Superalloys 2000 (Ninth International Symposium)*, 2000, pp. 255–261.
[8] P. Chapelle, C. Noël, A. Risacher, J. Jourdan, J. Jourdan, and A. Jardy, *IOP Conf. Ser. Mater. Sci. Eng.*, vol. 143, p. 012011, Jul. 2016.
[9] D. M. Shevchenko and R. M. Ward, *Metall. Mater. Trans. B*, vol. 40, no. 3, pp. 248–253, Jun. 2009.
[10] R. M. Ward, B. Daniel, and R. J. Siddall, *Proc. 2005 Int. Symp. Liq. Met. Process. Cast.*, 2005.
[11] A. Jardy, P. Chapelle, A. Malik, J.-P. Bellot, H. Combeau, and B. Dussoubs, *ISIJ Int.*, vol. 53, no. 2, pp. 213–220, 2013.
[12] R. M. Ward and M. H. Jacobs, *J. Mater. Sci.*, vol. 39, no. 24, pp. 7135–7143, Dec. 2004.
[13] C. R. Woodside and P. E. King, *Liq. Met. Process. Conf.*, 2009.
[14] M. Cibula, *Proc. Liq. Met. Process. Cast. Conf.*, pp. 25–30, Sep. 2017.

[15] M. Cibula, “Detection of Side-Arc Conditions in Vacuum Arc Remelting (VAR),” presented at the Titanium USA 2016 Conference, Pheonix, AZ, Oct-2016.
[16] C. R. Woodside and P. E. King, *2010 IEEE Instrumentation & Measurement Technology Conference Proceedings*, 2010, pp. 452–457.
[17] D. M. Shevchenko and R. M. Ward, *Metall. Mater. Trans. B*, vol. 40, no. 3, pp. 263–270, Jun. 2009.
[18] P. Chapelle, H. El Mir, J. P. Bellot, A. Jardy, D. Ablitzer, and D. Lasalmonie, *J. Mater. Sci.*, vol. 39, no. 24, pp. 7145–7152, Dec. 2004.
[19] K. Kelkar, “Theoretical Basis for MeltFlow-VAR-Version-50.” Innovative Research, Mar-2014.
[20] F. Zanner, R. Williamson, and R. Erdmann, *Proc. Int. Conf. Liq. Met.*, pp. 13–29, 2005.
[21] K. Pericleous, G. Djambazov, M. Ward, L. Yuan, and P. D. Lee, *Metall. Mater. Trans. A*, vol. 44, no. 12, pp. 5365–5376, Dec. 2013.
[22] A. Mitchell, *Mater. Sci. Eng. A*, vol. 413–414, pp. 10–18, Dec. 2005.
[23] W. Zhang, P. D. Lee, and M. McLean, *Metall. Mater. Trans. A*, vol. 33, no. 2, pp. 443–454, Feb. 2002.
[24] H. Kou, Y. Zhang, Z. Yang, P. Li, J. Li, and L. Zhou, *Int. J. Eng.*, vol. 12, no. 01, p. 7, 2012.